Proceedings of the 21st ICSMGE, Vienna, Austria, 14 – 19 June 2026. Pistrol, Adam & Schweiger (eds.)
Published by: ÖGG, Austrian Society for Geomechanics, Salzburg, Austria, ISBN 978-3-9503898-4-5
https://doi.org/10.53243/ICSMGE2026-2300

Understanding slip propagation of contact surfaces due to the non-uniform normal stress distribution using super/subloading surface friction model

Ryo Yasuike, Tomohiro Toyoda
Department of Civil and Environmental Engineering, Nagoya University, Japan, yasuike.ryo.z9@s.mail.nagoya-u.ac.jp

ABSTRACT: The boundary conditions for solid deformation analysis are given by either the Dirichlet boundary condition (prescribed displacements) or the Neumann boundary condition (prescribed loads), but actual contact surfaces exhibit frictional behavior causing boundary non-linearity accompanying a continuous transition between stick and slip states. In geotechnical engineering, it is essential to understand friction-induced phenomena such as negative friction. We have proposed the super/subloading surface friction model. The constitutive model describes the elasto-plasticity of a contact surface regarding the state in which the static friction coefficient is larger than the kinetic friction coefficient as the "structure" of friction coefficient and describing the decay and healing of the structure with an evolution rule for capturing state transition between static and kinetic frictions. In this study, we developed the dynamic elastic infinitesimal deformation analysis incorporating the proposed model into the contact force boundary and investigated the influence of the normal stress distribution at the contact surface on the global slip behavior under a simple shear condition. As a result, the frequency of slip occurrence, the amount of displacement and stress drop were strongly influenced by the normal stress. The results are consistent with the reduction tendency of the number of earthquakes with the increase of confining pressure known in seismology. As for the slip propagation, the slip on low normal stress area did not propagate to other areas due to capacity of the incremental load at the surrounding sliding surface. However, the slip on high normal stress area propagated through the entire surface because the large tangential stress drop exceeds the resistance of the surrounding area.

KEYWORDS: Friction, Elasto-plasticity, Dynamic Deformation analysis, Stick-slip, Slip propagation.

1 INTRODUCTION

In solid deformation analysis, the boundary conditions are set with either Dirichlet boundary conditions (prescribed displacements) or Neumann boundary conditions (prescribed loads). However, the response of a real contact surface is not so simple and presents with strong non-linearity. As examples of the phenomenon, the following can be given

- Non-stationarity of contact state (stick/slip state)

When a friction pile is pulled from the ground, it moves with the ground due to stick state on the contact surface (prescribed displacement). However, when the friction force on the contact surface exceeds the maximum static friction force, a slip occurs and kinetic friction force is applied (prescribed load). After that, when pulling out the pile stops, the contact surface returns to the stick state. Brake squeal and periodic earthquakes are also explained as vibration phenomenon (stick-slip phenomenon) caused by periodically repeating stick and slip state.

- History dependence

Negative friction occurs at the support piles when the ground settles under consolidation. This is a typical example of a phenomenon caused by the history dependence of the contact surface.

To evaluate such non-linear phenomena at the contact surface (e.g., temporal changes in the distribution of circumferential friction force, seismic mechanism at the fault plane), it is essential to develop a friction model that can describe the history of the contact surface and a deformation analysis method incorporating the model. The authors have proposed the super/subloading surface friction model which introduces the superloading surface concept (Asaoka et al., 2000) to the subloading surface friction model (Ozaki et al., 2007; Ozaki & Hashiguchi, 2010). In this elasto-plastic friction model, the transition between static and kinetic state is explained by the evolution rule of "degree of structure (adhesion)" which is an internal state variable presented the adhesion on the contact surface.

In this paper, we developed a new dynamic deformation analysis method considering friction using the model, we discussed how the normal stress distribution on the contact surface affects the slip behavior on a simple shear field.

2 MATERIALS AND METHODS

2.1 *Super/Subloading friction model*

This section outlines the super/subloading surface friction model. Details of the formulation are referred to Toyoda et al. (2024).

As shown in Figure 1, we assumed that the traction $\mathbf{f}$ is decomposed into the normal component $\mathbf{f}_n$ and the tangential component $\mathbf{f}_t$.Then, an isotropic Coulomb's friction criterion with kinetic friction coefficient was set as a normal sliding-yield surface on a traction space defined by f_n $(= \mathbf{f} \cdot \mathbf{n} > 0)$ and f_t $(= \|\mathbf{f}_t\|, \mathbf{f}_t = \mathbf{f} - \mathbf{f}_n)$. Here, $\mathbf{n}$ is the outward normal vector viewed from the main body (Figure 2). Next, the superloading-sliding surface was defined as the criterion plane of static friction at a position higher than the normal sliding-yield surface with a similarity ratio R^* $(\mu_k/\mu_s \leq R^* \leq 1$; $1/R^*, \mu_k, \mu_s$ represent the degree of structure, the kinetic friction coefficient and the static friction coefficient). Furthermore, the subloading-sliding surface was defined at a position similar to the superloading-sliding surface with a similarity ratio R $(0 < R \leq 1$; R represents the normal sliding ratio) The surface always passes through the current traction. Therefore, the normal sliding-yield surface, the superloading-sliding surface and subloading-sliding surface can be written as follows:

$$\text{Normal sliding-yield surface:} \quad \frac{f_t}{f_n} - \mu_k = 0, \tag{1}$$

$$\text{Superloading-sliding surface:} \quad \frac{f_t}{f_n} - \frac{1}{R^*}\mu_k = 0, \tag{2}$$

$$\text{Subloading-sliding surface:} \quad \frac{f_t}{f_n} - \frac{R}{R^*}\mu_k = 0. \tag{3}$$

By substituting $\mu = \mu_k/R^*$ to the evolution rule of the friction coefficient (Ozaki et al., 2007), the evolution rule of the degree of structure can be written as follows:

$$\dot{R}^* = \kappa \frac{R^{*2}}{\mu_k}\left(\frac{1}{R^*} - 1\right)^m \|\overline{\boldsymbol{v}}^p\| - \xi \frac{R^{*2}}{\mu_k}\left(1 - \frac{\mu_k}{\mu_s}\frac{1}{R^*}\right)^n, \tag{4}$$

where κ, m, ξ and n are non-negative material constants and defined in accordance with the previous paper (Toyoda et al., 2024). $\bar{\mathbf{v}}^p$ represents the plastic component of the sliding velocity $\bar{\mathbf{v}}$ ($=\bar{\mathbf{v}}^e + \bar{\mathbf{v}}^p$, $\bar{\mathbf{v}}^e$ represents the elastic component of sliding velocity). The first term is modeled the decrease of the friction coefficient from static to kinetic friction as the decay of structure on the contact surface due to the plastic sliding. The second term is modeled the increase of friction coefficient from kinetic to static friction as the healing of structure over time (Figure 3). Unlike Ozaki et al. (2007), and Ozaki & Hashiguchi (2010), who modeled the transition phenomenon between static and kinetic friction using the evolution rule of the friction coefficient, this model can explicitly express the change of "adhesion," which is the mechanism of friction, using the internal state variable R^*.

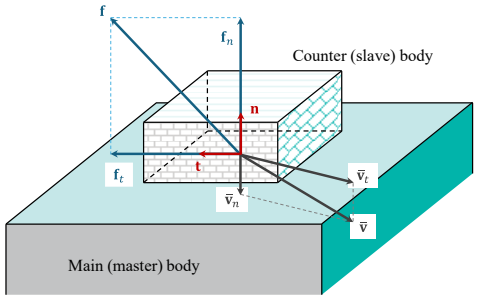

Figure 1. Decomposition of contact traction and sliding velocity (referred Ozaki et al. (2010) with additional description).

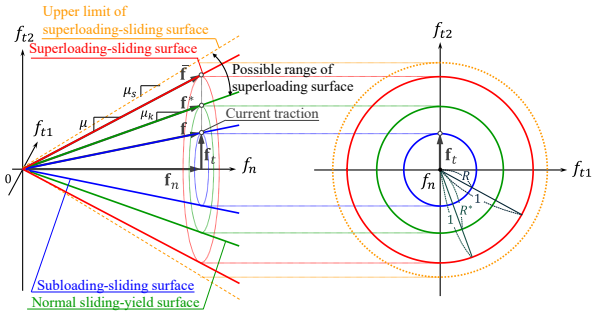

Figure 2. Superloading, subloading and normal yield surfaces (referred Ozaki et al. (2007), and Ozaki & Hashiguchi (2010) with additional description).

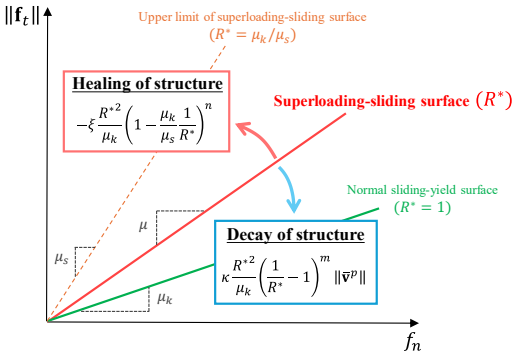

Figure 3. The transition of superloading-sliding surface.

The other basic equations (decomposition of sliding velocity, constitutive equation for elastic component, consistency condition, sliding flow law and evolution rule of R) are in accordance with the previous report (Toyoda et al., 2024). The plastic multiplier Λ (>0) which represents the magnitude of plastic slip and the constitutive equation using relative displacement rate are derived with the tangential unit vector $\mathbf{t}$ ($=\mathbf{f}_t/\|\mathbf{f}_t\|$) as follows:

$$\Lambda = \frac{\left(\alpha_n \frac{R}{R^*}\mu_k\mathbf{n} - \alpha_t\mathbf{t}\right)\cdot\bar{\mathbf{v}} - \xi R\left(1-\frac{\mu_k}{\mu_s}\frac{1}{R^*}\right)^n \mu_k f_n}{\alpha_t + r\frac{-\ln R}{R^*}\mu_k f_n - \kappa R\left(\frac{1}{R^*}-1\right)^m \mu_k f_n}, \tag{5}$$

$$\mathring{\mathbf{f}} = \begin{cases} \mathbf{C}^{ep}\bar{\mathbf{v}} + C^c\mathbf{t} & \ldots \text{loading} \quad (\bar{\mathbf{v}}^p \neq \mathbf{0}) \\ \mathbf{C}^e\bar{\mathbf{v}} & \ldots \text{unloding} \ (\bar{\mathbf{v}}^p = \mathbf{0})' \end{cases} \tag{6}$$

where

$$\mathbf{C}^{ep} = \mathbf{C}^e - \frac{\alpha_t\mathbf{t}\otimes\left(\alpha_n\frac{R}{R^*}\mu_k\mathbf{n} - \alpha_t\mathbf{t}\right)}{\alpha_t + r\frac{-\ln R}{R^*}\mu_k f_n - \kappa R\left(\frac{1}{R^*}-1\right)^m\mu_k f_n}, \tag{7}$$

$$C^c = \frac{\alpha_t\xi R\left(1-\frac{\mu_k}{\mu_s}\frac{1}{R^*}\right)^n\mu_k f_n}{\alpha_t + r\frac{-\ln R}{R^*}\mu_k f_n - \kappa R\left(\frac{1}{R^*}-1\right)^m\mu_k f_n}. \tag{8}$$

$\mathbf{C}^e = -\alpha_n\mathbf{n}\otimes\mathbf{n} - \alpha_t(\mathbf{I} - \mathbf{n}\otimes\mathbf{n})$ represents the second-order elastic tensor with $\mathbf{I}$ is the identity tensor, and the positive constants α_n, α_t are elastic moduli corresponding to the penalty coefficient in contact analysis. r is the positive parameter based on the revolution rule of R. The loading/unloading could be determined by checking a sigh of Λ in (5), i,e.,

$$\begin{cases} \Lambda > 0 \ldots \text{loading} & (\bar{\mathbf{v}}^p \neq \mathbf{0}) \\ \Lambda \leq 0 \ldots \text{unloading} & (\bar{\mathbf{v}}^p = \mathbf{0}) \end{cases}. \tag{9}$$

2.2 *Dynamic deformation method incorporating the model to contact force boundary condition*

This section outlines the formulation of the rate-type dynamic deformation introducing the contact force boundary (denoted S_c) as one of the boundary conditions to describe the stress transition on the contact surface in Figure 4. In this paper, the proposed model was applied to the boundary condition.

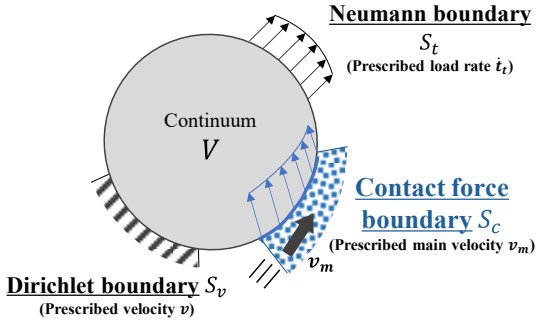

Figure 4. Boundary condition considering friction.

To focus on the non-linearity caused by friction, we conducted the infinitesimal elastic analysis which was not considered the elasto-plasticity of body and the finite deformation. This is why the co-rotational rate of traction $\mathring{\mathbf{f}}$ is equal to the material time derivative of traction $\dot{\mathbf{f}}$. Then the load rate boundary of the body was divided into Neumann boundary and contact force boundary in the following weak form of rate-type equation of motion:

$$\int_V \rho\ddot{\boldsymbol{v}}\cdot\delta\boldsymbol{v}\,dV + \int_V \dot{\boldsymbol{\sigma}}\cdot\delta\dot{\boldsymbol{\varepsilon}}\,dV = \int_V \dot{\boldsymbol{b}}\cdot\delta\boldsymbol{v}\,dV + \int_{S_t}\dot{\boldsymbol{t}}_t\cdot\delta\boldsymbol{v}\,dS + \int_{S_c}\dot{\boldsymbol{f}}_c\cdot\delta\boldsymbol{v}\,dS, \tag{10}$$

where $\rho, \dot{\boldsymbol{\sigma}}$ are the density and the stress rate of the body, $\dot{\boldsymbol{b}}$ is the object force velocity, $\dot{\boldsymbol{t}}_t$ is the prescribed stress rate on the Neumann boundary condition, and $\dot{\boldsymbol{f}}_c$ is the contact traction

rate on the contact force boundary. $\boldsymbol{v}, \delta\boldsymbol{v}, \delta\dot{\boldsymbol{\varepsilon}}$ is the displacement velocity of the counter body, an arbitrary function (but $\delta\boldsymbol{v} = \mathbf{0}$, on Dirichlet boundary S_v) and the virtual strain velocity. The third term on the right-hand side of (10) was formulated by applying the super/subloading surface friction model. Based on the friction constitutive Equation (6), the traction rate $\{\dot{\boldsymbol{f}}_c\}$ on the contact force boundary can be written as follows

$$\{\dot{f}_c\} = \begin{cases} [\mathbf{C}^{ep}]\{\bar{\boldsymbol{v}}^{\mathrm{N}}\} + \mathrm{C}^{\mathrm{c}}\{\boldsymbol{t}\} & \cdots \text{loading} \\ [\mathbf{C}^{e}]\{\bar{\boldsymbol{v}}^{\mathrm{N}}\} & \cdots \text{unloading} \end{cases}, \tag{11}$$

where $[\mathbf{C}^{ep}], [\mathbf{C}^{e}]$ are matrices based on the super/subloading surface friction model, and $\{\boldsymbol{t}\}$ is the tangential unit vector of the contact force boundary. The nodal sliding vector $\{\bar{\boldsymbol{v}}^{\mathrm{N}}\}$ on the element boundary surface is expressed as follows:

$$\{\bar{\boldsymbol{v}}^{\mathrm{N}}\} = \{\tilde{\boldsymbol{v}}^{\mathrm{N}}\} - \{\tilde{\boldsymbol{v}}^{\mathrm{N}}_{\mathrm{m}}\}, \tag{12}$$

where $\{\tilde{\boldsymbol{v}}^{\mathrm{N}}\}, \{\tilde{\boldsymbol{v}}^{\mathrm{N}}_{\mathrm{m}}\}$ are the displacement velocity of the counter body (unknown) and main body (known). Therefore, the integrand of third term on the right-hand side of the weak form of equation of motion is expressed as follows:

$$\begin{aligned} \dot{\boldsymbol{f}}_c \cdot \delta\boldsymbol{v} &= \{\delta\boldsymbol{v}^{\mathrm{N}}\}^{\mathrm{T}} \left\{ [\tilde{N}]^T \{\dot{\boldsymbol{f}}_c\} \right\} \\ &= \begin{cases} \{\delta\boldsymbol{v}^{\mathrm{N}}\}^{\mathrm{T}} \left\{ \begin{array}{r} [\tilde{N}]^T [\mathbf{C}^{ep}][\tilde{N}]\{\boldsymbol{v}^{\mathrm{N}}\} \\ -[\tilde{N}]^T [\mathbf{C}^{ep}][\tilde{N}]\{\boldsymbol{v}^{\mathrm{N}}_{\mathrm{m}}\} \\ +\mathrm{C}^{\mathrm{c}}[\tilde{N}]^T\{\boldsymbol{t}\} \end{array} \right\} & \cdots \text{loading} \\ \{\delta\boldsymbol{v}^{\mathrm{N}}\}^{\mathrm{T}} \left\{ \begin{array}{r} [\tilde{N}]^T [\mathbf{C}^{e}][\tilde{N}]\{\boldsymbol{v}^{\mathrm{N}}\} \\ -[\tilde{N}]^T [\mathbf{C}^{e}][\tilde{N}]\{\boldsymbol{v}^{\mathrm{N}}_{\mathrm{m}}\} \end{array} \right\} & \cdots \text{unloading} \end{cases}, \end{aligned} \tag{13}$$

Note that the displacement velocities of the counter body and the main body ($\{\tilde{\boldsymbol{v}}^{\mathrm{N}}\}, \{\tilde{\boldsymbol{v}}^{\mathrm{N}}_{\mathrm{m}}\}$) on the contact force boundary are described by expanding the displacement velocity ($\{\boldsymbol{v}^{\mathrm{N}}\}, \{\boldsymbol{v}^{\mathrm{N}}_{\mathrm{m}}\}$) at each node of the element. $[\tilde{N}]$ represents a matrix based on the shape function of the finite element method. Considering the arbitrariness of $\{\delta\boldsymbol{v}\}$, the discrete expression of the equation of motion can be expressed as follows:

$$\mathrm{M}\{\ddot{\boldsymbol{v}}^{\mathrm{N}}\} + (\mathrm{K} - \mathrm{K_c})\{\boldsymbol{v}^{\mathrm{N}}\} = \{\dot{\boldsymbol{f}}^{0}\} + \{\dot{\boldsymbol{f}}^{\mathrm{c}}\}, \tag{14}$$

where M, K, and $\{\dot{\boldsymbol{f}}^{0}\}$ are the condensed global mass matrix, global stiffness matrix, and global nodal force vector respectively. $\mathrm{K_c}$ and $\{\dot{\boldsymbol{f}}^{\mathrm{c}}\}$ are matrix and load vector based on the super/subloading surface friction model. As for the time integration, Equation (14) was implicitly solved using the Wilson's θ method assuming linearity of jerk (material time derivative of acceleration) refer to Noda et al. (2008). The traction force was calculated as the Gauss integral of contact stress, which is interpolated with first-order isoparametric element. The formulas for the time integration of variables (contact stress, degree of structure, normal sliding ratio) defined at each Gauss point on the contact surface were also implicitly integrated with the trapezoidal rule. Thus, this dynamic deformation analysis made it possible to consider the transition on the contact surface (stick/slip state).

3 INFLUENCE OF NON-LINEAR NORMAL DISUTRIBUTION TO SLIP BEHAVIOR

3.1 *Introduction*

In seismology, a record of the number of earthquakes at each depth in a subduction zone, as shown in Figure 5, indicates that slip occurs less frequently at deeper depths. This shows that the large and low-frequency slip occurs at deeper depths due to the high confining pressure (effective normal stress), while small and high-frequency slip occurs at shallower depths due to the low confining pressure. In this paper, we discussed the influence of the non-uniform normal stress distribution on the slip behavior due to confining pressure under a simple shear condition.

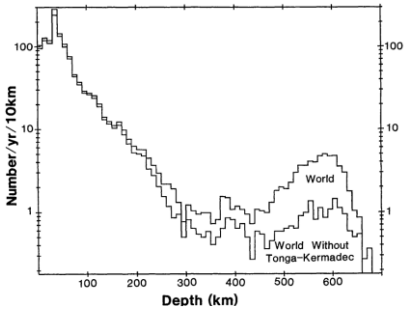

Figure 5. Depth distribution of slip frequency (Frohlich, 1989).

3.2 *Analysis condition*

As shown in Figure 6, we set of a 10-meter wide and 1-meter high an isotropic linear elastic body (10 elements) in 2D plain strain condition. The top surface was assumed to be completely fixed, and the bottom surface was assumed to be the contact force boundary. A horizontal displacement velocity $v_{m,x}$, 0.001 m/s, was applied to the base body with the bottom surfaces of the analysis domain. The initial normal stress distribution was triangular, as shown in Figure 7. To evaluate the influence of the initial normal stress distribution to slip behavior, we assumed that the initial normal stress distribution on the bottom surface on the contact force boundary was kept constant during shear deformation. The parameters and initial conditions used are shown in Table 1, 2 and 3.

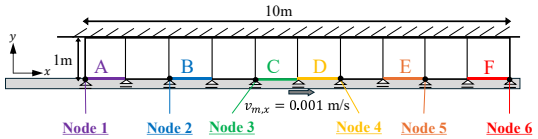

Figure 6. Finite element mesh.

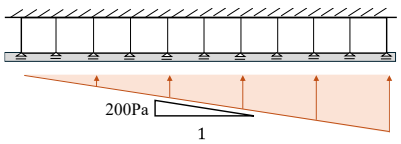

Figure 7. Normal stress distribution.

Table 1. Parameters about the super/subloading surface friction model.

Parameter	Symbol	Value	Unit
The static friction coefficient	μ_s	0.4	-
The kinetic friction coefficient	μ_k	0.2	-
Elastic modulus [normal/tangential]	α_t, α_n	1000	kPa/m
Parameter for evolution rule of R	r	100	1/m
Parameter for evolution rule of R^*	κ	10	1/m
Parameter for evolution rule of R^*	m	1	-
Parameter for evolution rule of R^*	ξ	0.1	1/s
Parameter for evolution rule of R^*	n	1	-

Table 2. Elastic material parameters.

Parameter	Symbol	Value	Unit
Young's modulus	E	1.0×10^{3}	N/m^2
Poisson's ratio	ν	0.0	-
Density	ρ	1.0	g/cm^3

Table 3. Initial condition.

Parameter	Symbol	Value	Unit
Initial degree of structure	$1/R^*$	2.0	-
Initial tangential traction stress	f_{t0}	1.0×10^{-7}	Pa

3.3 *Results and discussion*

The time histories of the horizontal displacements at Nodes 1~6, the total friction forces (area integration of the horizontal component of the contact stress) and the degree of structure at Segments A~F are shown in Figure 8 and 9. Figure 8 showed that there was a clear difference of slip frequency and the amount of slip depending on the horizontal position of contact surface. At the left end (Node 1) where the normal stress is small, small slips occurred at a high frequency (5 times in 1000 s from the beginning) and the next slip occurred before the structure of the contact surface has not fully recovered (R^* $\simeq$1.5). On the other hand, at the right end (Node 6) where the normal stress is high, large slip occurred at a low frequency (once in 1000 s from the beginning), and the next slip occurred when the structure of the contact surface has recovered enough ($R^*\simeq$1.9). These results were consistent with the findings indicated by Frohlich (1989) that the frequency of earthquake occurrence decreases with depth. As for the slip propagation, the slip at the left side of the contact surface (Segments A and B), where the normal stress is small, did not propagate toward to the central region (time zone [1] in Figure 9), while the slip at the right side of the contact surface (Segments E and F), where the normal stress is large, always accompanied the slip at the left side (time zone [2] in Figure 9). Focusing on the time zone [1] in Figure 9, the slip did not propagate to the entire contact surface because the frictional force drop associated with the slip in regions A and B was balanced by the frictional resistance of the surrounding region (mainly region C). On the other hand, focusing in the time zone [2] in Figure 9, the slip propagated to the left edge of the contact surface without staying there because the frictional resistance in the surrounding area was not able to support the increased load. In other words, the slip in the region with small normal stress remained localized, while the slip in the region with large normal stress propagates to the surrounding area, triggering the slip on the entire contact surface.

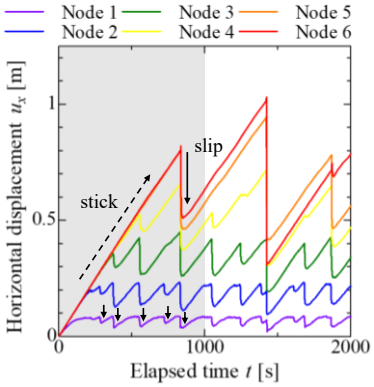

Figure 8. The time history of the horizontal displacements.

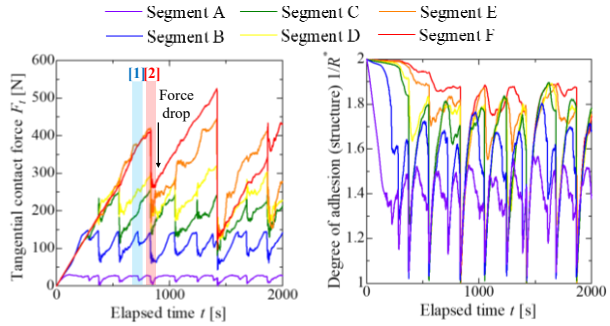

Figure 9. The time histories of the tangential contact forces and the degree of structure.

4 CONCLUSION AND FUTURE WORKS

In this paper, we developed the rate-type dynamic infinitesimal deformation analysis incorporating the friction model proposed by us to the contact force boundary. We discussed the influence of the normal stress distribution at the contact surface on slip behavior under a simple shear condition with the analysis. The results showed that the frequency of slip is lower, and the slip displacement and friction force drop is larger at the contact surface where the normal stress distribution is larger. These are consistent with the variety of frequency of cyclic earthquake occurrence due to confining pressure known in seismology.

We plan to apply the model to the boundary conditions of soil-water coupled analysis considering material non-linearity (elasto-plasticity) and geometric non-linearity (finite deformation) in addition to boundary non-linearity. Then, we plan to conduct research with the developed method to understand friction-related engineering problems such as negative friction and vibration during pile penetration/extraction, and to model the mechanism of earthquake generation on a fault plane.

5 ACKNOWLEDGEMENTS

In conducting this study, we also had various discussions with Dr. Toshihiro Noda, Professor of Nagoya University. This work was supported by JSPS KAKENHI (grant number 22H01586). This work was also financially supported by JST SPRING, Grant Number JPMJSP2125 and the "THERS Make New Standards Program for the Next Generation Researchers."

6 REFERENCES

Asaoka, A., Nakano, M., and Noda, T. 2000. Superloading yield surface concept for highly structured soil behavior. *Soils and foundations*, 40(2), 99-110.

Frohlich, C. 1989. The nature of deep-focus earthquake. *Annual Review of Earth and Planetary Sciences*, 14, 227-54.

Noda, T., Asaoka, A., and Nakano. M. 2008. Soil-water coupled finite deformation analysis based on a rate-type equation incorporating the SYS Cam-clay model. *Soils and foundations*, 48(6), 771-90.

Ozaki, S., Hashiguchi, K., and Chen, D-H. 2007. Study on stability of stick-slip motion by the time-dependent constitutive equation for friction. *Journal of applied mechanics*, 10, 445-55

Ozaki, S., Hashiguchi, K. 2010. Numerical analysis of stick-slip instability by a rate- dependent elastoplastic formulation for friction. *Tribology international*, 43(11), 2120–33.

Toyoda, T., Yasuike, R., and Noda, T. 2024. Super/sub-loading surface model for constitutive equation of friction. *Tribology international*, 191, 109080.